Environmental Science & Technology

pubs.acs.org/est

Article

Biodefluorination of Unsaturated Perfluorinated Carboxylic Acid by Anaerobic Digestion Sludge: Who and How?

Qiu-Jin Xu, He-Ping Zhao,* Carolyn R. Cornell, Chuncheng Wu, Sarah Glass, Jacques Mathieu, and Pedro J. J. Alvarez

Cite This: *Environ. Sci. Technol.* 2025, 59, 21567−21578

Read Online

ACCESS | Metrics & More | Article Recommendations | Supporting Information

ABSTRACT: Per- and polyfluoroalkyl substances (PFAS) are widespread environmental pollutants that are notoriously recalcitrant to biodegradation. We explored the biotransformation and defluorination of *(E)*-perfluoro-4-methylpent-2-enoic acid (PFMeUPA), a perfluorinated compound with diverse C−F bonds, using municipal anaerobic digestion sludge. Defluorination was stimulated with various substrate amendments and characterized by the release of fluoride (F^-) and the formation of corresponding byproducts. Methanol, formate, acetate, and lactate enhanced reductive defluorination as electron donors. However, the addition of vitamin B_{12} (a cobalt−corrin complex), which commonly enhances reductive dehalogenation, had no effect. The methanogenesis inhibitor 2-bromoethanesulfonate had no significant effect, ruling out direct participation by methanogens. After 80 days of incubation, *Sulfurospirillum* and *Asaccharospora* exhibited significantly higher relative abundance in all substrate-amended treatment groups compared to those in both the original inoculum and control groups (no substrate or no PFAS added), indicating selective enrichment under defluorinating conditions. Comparative analysis of genomes that were enriched relative to the inoculum and that harbored the fluoride exporter *crcB* gene (n = 23) versus genomes lacking *crcB* (n = 233) revealed two novel defluorinating candidates belonging to the *Sulfurospirillum* genus (A_bin.69 and M_bin.68). Overall, these findings advance the understanding of anaerobic PFAS biodegradation and suggest *crcB* as an auxiliary biomarker to discover putative defluorinating species.

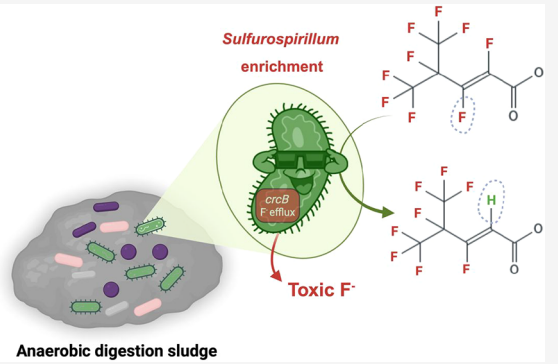

KEYWORDS: *anaerobic digestion, perfluorinated carboxylic acid, anaerobic PFAS degradation*

1. INTRODUCTION

Per- and polyfluoroalkyl substances (PFAS) are extensively used in a wide range of industrial and commercial applications, including firefighting foams and food packaging materials.[1−3] This has resulted in widespread environmental pollution, which raises significant public and environmental health concerns due to their mobility, extreme persistence, and potential to bioaccumulate.[4,5] Many countries have enacted highly stringent limits for PFAS concentrations in drinking water,[6,7] which has motivated significant activity on treatment process innovation.

Physicochemical methods for PFAS degradation, such as mechanochemical destruction,[8−10] hydrothermal alkaline hydrolysis,[11,12] thermal pyrolysis,[13,14] UV/photocatalysis,[15−17] or electrochemical destruction,[18−20] usually require relatively high energy inputs and/or harsh chemical agents. Thus, there is significant interest in exploring microbial defluorination as a potential cost-effective alternative to cleaving C−F bonds under mild conditions. Although PFAS are generally recalcitrant to microbial transformation under various conditions,[21−23] microbial cleavage of C−F bonds has been reported. An *Acidimicrobium* sp. strain A6 enrichment was shown to defluorinate PFOA/PFOS initially added at 0.1 and 100 mg/L.[24−27] Another study reported that a consortium degraded ∼9% of PFOA (initial concentration 5 mg/L) after 10 months of incubation.[28] Similarly, 40% of PFOS in contaminated soil was removed after 45 days, but without direct evidence of microbial reductive defluorination.[29] These studies offered limited molecular evidence directly linking microbial activities to C−F bond cleavage,[30] and the precise defluorination mechanisms remain unresolved.

Microbial defluorination is better understood for some shorter-chain perfluorinated compounds or polyfluorinated compounds, which have been observed under both aerobic and anaerobic conditions.[31−33] The unsaturated perfluorinated compound, *(E)*-perfluoro-4-methylpent-2-enoic acid (PFMeUPA, $(CF_3)_2CFC{=}CFCOOH$), was defluorinated by a

Received: May 20, 2025
Revised: September 19, 2025
Accepted: September 22, 2025
Published: October 2, 2025

https://doi.org/10.1021/acs.est.5c06744
Environ. Sci. Technol. 2025, 59, 21567−21578

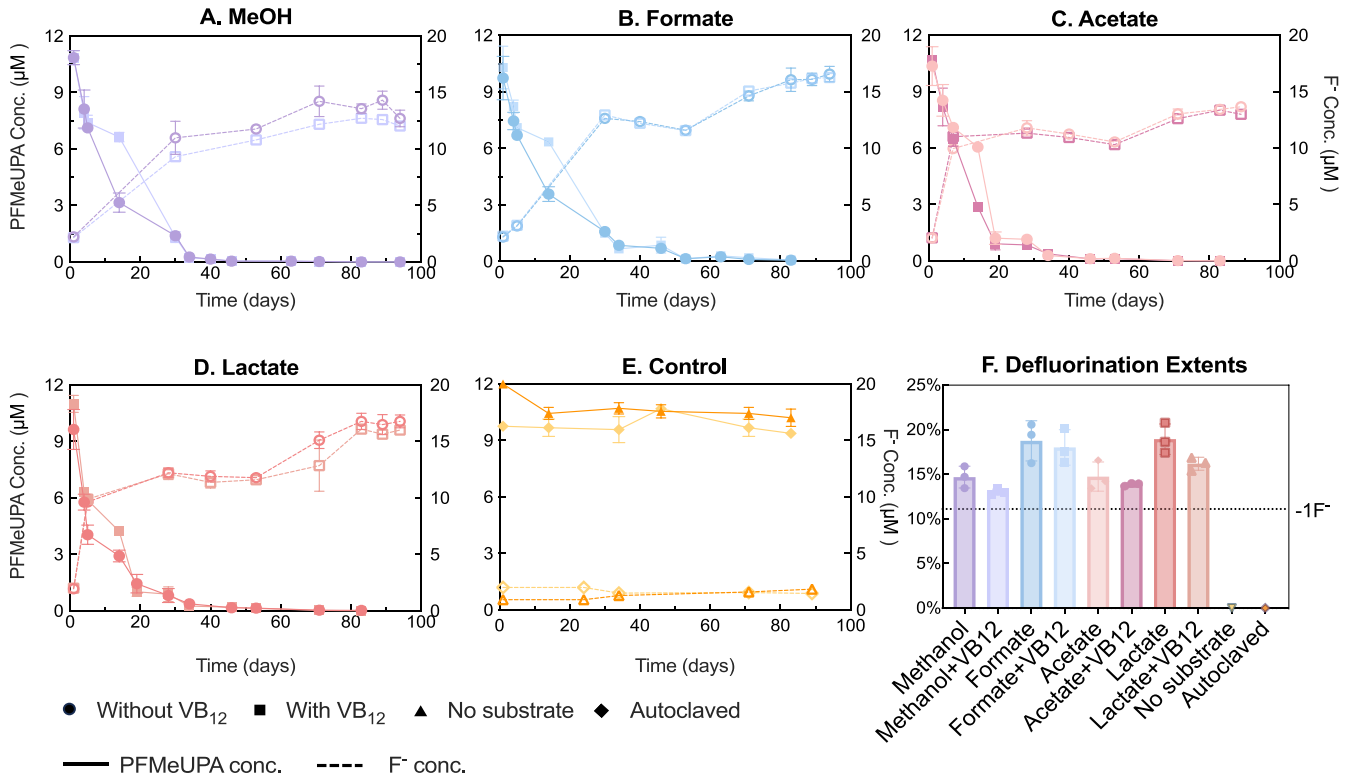

Figure 1. PFMeUPA removal and fluoride release in anaerobic sludge with different treatment amendments: (A) methanol, (B) formate, (C) acetate, (D) lactate, (E) no substrate control and autoclaved control. Panel F compares defluorination extent across treatments. Defluorination extent is normalized to the theoretical maximum defluorination percent. Error bars denote ± one standard deviation from the mean of triplicate biological replicates.

commercial dechlorinating consortium,[32] and *Acetobacterium* spp. were identified as defluorinating bacteria that possess two key molecular determinants: (i) the *crcB*-encoded fluoride efflux system, which mitigates intracellular fluoride toxicity, and (ii) an electron-bifurcating caffeate reductase complex that generates the ultralow redox potential required for C−F bond cleavage.[34] These studies demonstrated the potential for C−F bond cleavage under anaerobic conditions, but critical gaps remain in advancing the predictive understanding of these processes and translating them into robust, practical technologies.

Municipal wastewater treatment plants are common sinks of water pollutants, including PFAS.[35,36] Yet, very few studies have investigated PFAS biodefluorination in real-world wastewater treatment systems.[37] The fate of PFAS in anaerobic digestors requires special attention due to growing concerns about their presence in the resulting biosolids that are commonly used as nutrient-rich and inexpensive soil amendments.[38] Furthermore, anaerobic digestion sludge (DS) represents functionally diverse microbial consortia capable of degrading recalcitrant organic pollutants,[39−41] which encourages assessing their PFAS transformation capabilities. Here, we incubated DS with PFMeUPA and stimulated reductive defluorination with different electron donors. By employing in-depth community- and gene-level analyses, we identified novel putative defluorinating species and pathways to advance mechanistic understanding of the role of municipal anaerobic processes in PFAS pollution control.

2. MATERIALS AND METHODS

2.1. Chemicals. The standard compound (*E*)-perfluoro(4-methylpent-2-enoic acid) (PFMeUPA, 99% purity, CAS No. 10322989−6) was purchased from SynQuest Laboratories (Alachua, FL) and used without further purification. A 1000 mg/L stock solution was prepared anaerobically in autoclaved Milli-Q water in a 200 mL serum bottle and stored at 4 °C until use. Methanol (HPLC grade, ≥99.9% purity), sodium acetate (anhydrous, 99% purity), sodium formate (ACS grade, 99% purity), and sodium lactate (ACS grade, ≥98% purity) were sourced from Thermo Scientific Chemicals. Anaerobic 1000 mM stock solutions of these substrates were also prepared in autoclaved Milli-Q water in 200 mL serum bottles and stored at 4 °C until use.

2.2. Batch Experiments of Defluorination. Batch tests were conducted in 125 mL serum bottles using a mineral salt medium (Table S1). The medium was autoclaved at 121 °C for 20 min for two cycles. Anaerobic digestion sludge (10 mL, 12.1 mg VSS/mL), sampled from a municipal wastewater treatment plant in Houston, Texas (pretreatment detailed in SI), was inoculated into 90 mL of the mineral salt medium. The bottles were deoxygenated by sparging with helium (>99.99% purity) for 5 min and sealed with rubber stoppers. Resazurin (1 mg/L) was added as an oxygen indicator. In the treatment groups, 10 μM PFMeUPA was added along with 5 mM of substrates: methanol (group M), sodium formate (group F), sodium acetate (group A), and sodium L-lactate (group L). Additional groups included 100 μg/L vitamin B12 (M_VB12, F_VB12, A_VB12, L_VB12), which was periodically replenished. These four distinct substrates were resupplied upon depletion for all groups to sustain robust

https://doi.org/10.1021/acs.est.5c06744
Environ. Sci. Technol. 2025, 59, 21567−21578

biomass growth and maintain metabolic activity throughout the defluorination process.

The control experiments included: (1) abiotic (no sludge), (2) autoclaved (sterilized postinoculation), (3) no substrate (NS), (4) no PFMeUPA with formate (FNF), and (5) headspace with 20 mL hydrogen (H_2, >99.9% purity) at room temperature under 1 atm. Details are provided in Table S2. During incubation, 2 mL samples were taken once a week to measure substrate (0.1 mL), parent organofluorine compound (0.01 mL), and fluoride ions (1.5 mL) until no further fluoride ion accumulation was observed (~12 weeks). Samples were centrifuged at 16,000*g* (4 °C, 30 min), with supernatants stored at 4 °C and cell pellets frozen at −80 °C for extraction. All experiments were incubated at 35 ± 1 °C in the dark without shaking and conducted in triplicate.

2.3. Methanogen Inhibition Batch Experiments. Whether methanogens played a direct role in defluorination was investigated by repeating tests in the presence of the methanogenesis inhibitor bromoethanesulfonate (BES). For these tests, 10 mL of the mixed cultures were transferred into fresh mineral medium (as previously described), 100 μM PFMeUPA was added to the new treatments, and 5 mM methanol (M_N), sodium formate (F_N), sodium acetate (A_N), or sodium L-lactate (L_N) were added as electron donors. BES (10 mM), a specific inhibitor of methyl-coenzyme M reductase,[42] was added to parallel groups (M_BES, F_BES, A_BES, L_BES). To confirm inhibition of methanogenesis, methane concentration was measured as described in Supporting text 2. Controls were established as in the first round. Sampling and incubation procedures followed the same protocol used for the initial batch. All experiments were conducted in triplicate.

2.4. Fluoride Ion Measurement by Ion-Selective Electrode Method and by IC. Fluoride ion (F^-) concentration in the sample supernatant was measured using an ion-selective electrode (ISE, Cole-Parmer) connected to a pH/ISE benchtop multiparameter meter (Orion Versa Star Pro, Thermo Scientific). An equal volume of total ionic strength adjustment buffer (TISAB II, Cole-Parmer) was added to 1.5 mL of the sample supernatant, and the F^- concentration was determined using the ISE and multiparameter meter. The ISE was calibrated for each measurement according to the manufacturer's instructions. The limit of quantification (LOQ) for ISE was 0.02 mg/L (~1 μM) F^-. Simultaneously, ion chromatography was used to validate ISE measurements as detailed in Supporting text 3.

The defluorination extent was calculated using the following equation

$$\text{defluorinaton extent (\%)} = \frac{C_{t\text{-fluoride}}}{9 \times (C_{0\text{-PFMeUPA}} - C_{t\text{-PFMeUPA}})} \times 100\%$$

where $C_{t-\text{fluoride}}$, $C_{0-\text{PFMeUPA}}$, and $C_{t-\text{PFMeUPA}}$ represent the fluoride concentration at time t, the initial PFMeUPA concentration, and the PFMeUPA concentration at time, respectively. In Figure 1F, we chose t = 89 days. The factor of 9 in the denominator corresponds to the maximum number of fluorine atoms per PFMeUPA molecule, as determined by its chemical structure.

2.5. Liquid Chromatograph Coupled Triple Quadrupole Mass Spectrometer (LC-TQ/MS). The parent compound PFMeUPA was quantified using an Agilent 1290 Infinity II liquid chromatography system coupled with a 6740 triple quadrupole mass spectrometer (TQ-MS) equipped with a jet stream electrospray ionization (ESI) source. Analysis was conducted at Rice University's Shared Equipment Authority. For liquid chromatography (LC), a 20 μL sample was injected onto a ZORBAX Eclipse Plus C18 column (2.1 mm × 5 mm, 1.8 μm) and eluted with 20 mM ammonium acetate (A) and methanol (B) at a flow rate of 0.4 mL/min. The LC gradient was as follows: 25% A (0−2 min), linear decrease to 0% A (2−7.5 min), and 100% B (7.5−10 min). The TQ-MS was operated in full-scan mode with negative ionization, scanning from m/z 50 to 750 at a resolution of 70,000 at m/z 200. The limit of quantification (LOQ) for PFMeUPA was 0.1 ppb, defined as the lowest concentration of calibration standards with less than 20% variation.

2.6. Transformation Products Identification. Nontargeted screening of transformation products (TPs) was performed using an Agilent 1290 Infinity II liquid chromatography system coupled with a 6546 quadrupole time-of-flight mass spectrometer (LC-QTOF). The LC conditions were identical to those used for parent compound analysis. The mass spectrometer operated in "Data Independent All Ions Fragmentation" mode with all ions passing through the Q-TOF collision cell under negative ionization polarity. Data from samples under the same treatment were analyzed collectively. All acquired data were processed using Agilent MassHunter Qualitative Analysis software (Version 12).

2.7. DNA Extraction and 16S rRNA Nanopore Sequencing. Total genomic DNA was extracted from groups M, F, A, and L, FNF (Formate_no_PFAS), and NS (No_substrate) sampled on day 80, and the initial inoculum (O) using the PowerSoil DNA Isolation Kit (Qiagen). The quality and quantity of the DNA were determined by using a NanoDrop 2000 spectrophotometer (Thermo Scientific). The 16S rRNA gene from 7 samples was amplified using Oxford Nanopore's 16S Barcoding Kit 1−24, with universal primers 27F and 1492R,[63] followed by adaptor ligation using the NEBNext Quick Ligation Module. Amplicons were purified with AMPure XP beads and pooled in equimolar concentrations for library preparation. The pooled library was loaded onto a MinION flow cell (R9.4.1) and sequenced on the MinION Mk1B device controlled by MinKNOW software. Sequencing data (90888−105811 raw PEreads) were basecalled using Guppy, demultiplexed via EPI2ME, and analyzed using *Situseq*[43] with taxonomic classification performed against the Silva 138.1 database.[44−46]

2.8. Metagenomic Sequencing and Analyses. DNA extracted from groups M, F, A, L, and O, as mentioned above, was used for library preparation using the Illumina TruSeq DNA Nano Library Prep Kit. The libraries were sequenced on the Illumina HiSeq X platform (2 × 150 bp), generating between 76.8 and 108.2 million reads per sample. All sequencing data were deposited in the Sequence Read Archive (SRA) under BioProject accession number SUB15332846. Raw data quality was assessed using FastQC (http://www.bioinformatics.babraham.ac.uk/projects/fastqc/), and Trimmomatic (version 0.38) was employed for trimming or removing low-quality reads using default parameters.[47] Postquality control reads were assembled separately and coassembled into contigs using MEGAHIT.[48] Contigs shorter than 500 bp were excluded, and Metabat followed by CheckM, was used to bin the qualified contigs and evaluate the quality of metagenome-assembled genomes (MAGs).[49,50] The relative

https://doi.org/10.1021/acs.est.5c06744
Environ. Sci. Technol. 2025, 59, 21567−21578

abundance of MAGs was calculated by mapping quality-filtered reads to contigs longer than 500 bp, using the BBmap (https://sourceforge.net/projects/bbmap/). The open reading frames (ORF) were predicted using Prodigal v2.6.3[51] and annotated using EGGNOG-mapper[52] with HMM search,[53] DIAMOND alignment,[54] and MMseq2[55] against the eggNOG database.[52,56] The genome-based analysis was also first annotated with Prodigal v2.6.3,[51] and functional annotations were predicted using Kofamscan with KOfam HMM set r02_18_2020.[57]

2.9. Functional Enrichment Analysis. To further investigate potential defluorination-associated genes, Fisher's exact tests were performed using the fisher.test function in R (v4.2.1)[58] to compare the presence or absence of each KEGG Orthology (KO) term between positive and negative genomes. We first identified 52 MAGs encoding *crcB* genes, among which 23 exhibited enrichment following incubation with PFMeUPA in the treatment groups. These 23 MAGs were designated as the positive group, while the remaining 23 MAGs (n = 233) were considered as the negative (control) group. Even though *crcB* does not code for defluorination, this enrichment analysis aimed to identify taxonomic genomes associated with defluorination because *crcB* endows critical resistance to intracellular fluoride production during PFMeUPA defluorination. Initial profiling detected 6,684 KEGG Orthology (KO) groups across all 256 genomes. After quality filtering to retain only those present in at least 20 genomes, 3384 KO groups were included in the statistical analysis. Note that this KO-based approach has the limitation of excluding genes with uncharacterized or unknown functions. All p-values were FDR-adjusted for multiple testing (p-adjust function, threshold = 0.05). KOs were assigned to broader functional categories as in Diamond et al.[59]

3. RESULTS AND DISCUSSION

3.1. Various Electron Donors Enhanced PFMeUPA Defluorination by Anaerobic Digestion Sludge. Anaerobic digestion sludge was incubated with 10 μM PFMeUPA and amended with 5 mM methanol, formate, acetate, or lactate as electron donors (designated groups M, F, A, and L). All groups achieved over 99% degradation of PFMeUPA within 40 days, leading to the accumulation of fluoride ions at ∼ 15 μM (Figure 1A−D), representing 14.7 ± 1.2% (M), 18.8 ± 2.2% (F), 14.8 ± 1.6% (A), and 19.0 ± 1.7% (L) of the theoretical maximum possible defluorination extent. Amendment with 20 mL (0.82 mmol) of H_2 resulted in 40.1 ± 11.4% PFMeUPA removal and ∼5.9% defluorination within 92 days (Figure S2A). This lower performance is possibly due to low hydrogen solubility.[60] Carbon sources were consumed concurrently with PFMeUPA degradation (Figure S1). No PFMeUPA removal or fluoride release was observed in controls with either no carbon sources or autoclaved sludge (Figure 1E), excluding abiotic PFMeUPA degradation.

Lactate was the most favorable substrate and drove PFMeUPA biodegradation at a rate of 1.63 ± 0.26 μmol·d^{-1}, which was significantly higher (p < 0.05) than with other substrates (Figure S2B). This rate is higher than that reported for the dechlorinating consortium KB1 (∼0.47 μmol·d^{-1}),[32] though a comparison of biomass-normalized specific rates is not possible since the KB1 concentration was not reported in that study. A second round of PFMeUPA testing showed repeatable complete PFMeUPA degradation within 30 days (Figure S11), suggesting that the enriched consortia possess sustained defluorination capability. Whereas these data clearly demonstrate biological defluorination, further research is needed to determine whether PFMeUPA played a metabolic role (e.g., served as a terminal electron acceptor in a respiratory dehalorespiration process to generate metabolic energy), or defluorination was a fortuitous cometabolic process without a clear energetic benefit to bacteria. However, halorespiration processes typically exhibit a relatively high fraction of the electron donor consumption coupled to reductive dichlorination.[61] Given the much higher concentration of consumed electron donors and lower PFMeUPA (e.g., 6.20 ± 0.23 mmol lactate versus 10.85 ± 0.38 μmol PFMeUPA), it is more likely that PFMeUPA was transformed cometabolically.

We also investigated the potential of vitamin B_{12} to enhance PFMeUPA defluorination. B_{12} is known to play a pivotal role in microbial reductive dechlorination, where it functions as both a cofactor and catalyst to facilitate electron transfer to chlorinated compounds, thereby enhancing the activity of organohalide-respiring bacteria (OHRB).[62−64] B_{12} has also been reported to enhance reductive defluorination of branched perfluoroalkyl acids like perfluoro-3,7-dimethyloctanoic acid ($PFMe_2OA$) at elevated temperatures (70 °C).[65,66] However, surprisingly, B_{12} supplementation showed no significant enhancement in either PFMeUPA degradation or fluoride release (Figure 1A−D). Although PFMeUPA contains structurally similar branched C−F bonds to $PFMe_2OA$, our results suggest that B_{12} could not overcome the bond cleavage energy under ambient conditions. This implies that the C−F bond cleavage in PFMeUPA may proceed via a distinct enzymatic pathway that does not require VB_{12} as a cofactor, or that the high strength of C−F bonds compared to C−Cl bonds may render VB_{12} ineffective as a standalone catalyst under ambient conditions.

We observed substantial methane production during incubation (Figure S3). This could imply that methanogens participated in the defluorination process or conversely hindered it by competing for electrons that would otherwise be used for PFMeUPA reductive defluorination. To discern whether methanogens enhanced or inhibited defluorination, we inhibited methanogenesis with BES (Figure S4), which had no significant effect on the degradation of ∼80 μM PFMeUPA (Figure S5). First-order degradation rate coefficients were determined for all of the treatments (Table S4). For groups F, F_BES, L, and L_BES, there was little difference in PFMeUPA degradation rates with or without BES, with a k value of 0.050 ± 0.017, 0.050 ± 0.012, 0.023 ± 0.006, and 0.028 ± 0.009 d^{-1}, respectively. However, groups M, M_BES, A, and A_BES with a k value of 0.027 ± 0.10, 0.014 ± 0.007, 0.033 ± 0.013, and 0.019 ± 0.007 d^{-1}, respectively, showed a slightly higher PFMeUPA degradation rate in noninhibited groups and no significant difference in F^- release. Thus, methanogens did not play a direct significant role in PFMeUPA degradation, as previously reported for *Methanosarcina barkeri* pure cultures.[34]

3.2. C−F Bond Cleavage Was Initiated at the Unsaturated Carbon of PFMeUPA. PFMeUPA transformation products (TPs) were identified by LC-QTOF/MS. A major TP has a m/z of 256.9859 (TP256) and its composition includes fragments at m/z 212.99 (C_5HF_8), 192.98 (C_5F_7), and 168.98 (C_3F_7) (Figure S7). The chromatogram shows a single symmetric peak for TP256 (without a shoulder peak), indicating negligible stereoisomers with the same m/z (256.9856 ± 5 ppm). Furthermore, the α-C of PFMeUPA was recently reported to be preferentially

https://doi.org/10.1021/acs.est.5c06744
Environ. Sci. Technol. 2025, 59, 21567−21578

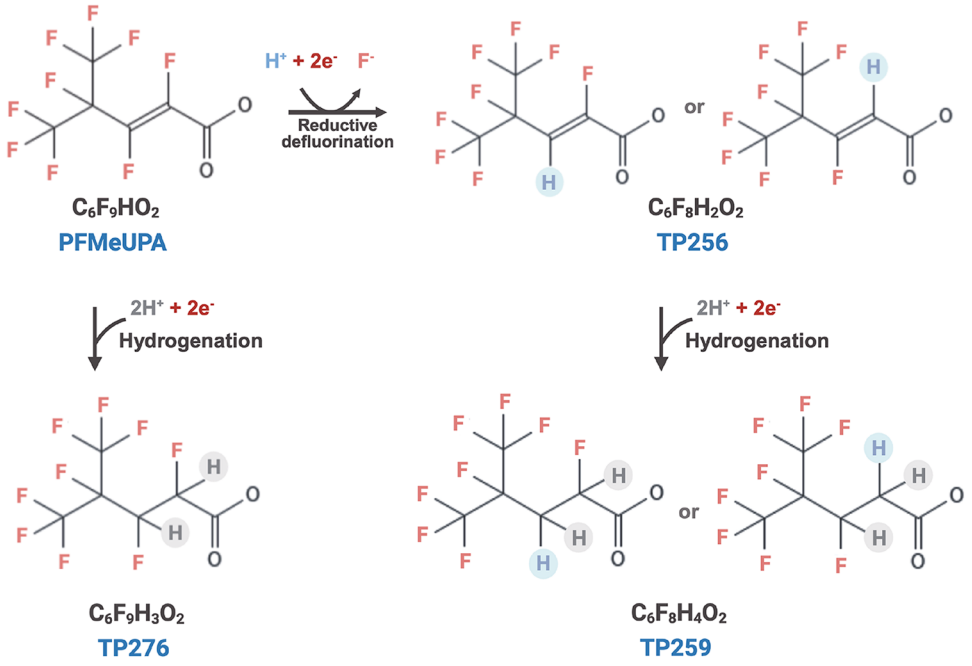

Figure 2. Proposed anaerobic biotransformation pathway of PFMeUPA. Transformation products were identified in the aqueous phase using liquid chromatography coupled with quadrupole time-of-flight mass spectrometry (LC-QTOF/MS). Plausible structures were assigned based on: (i) exact mass measurements (mass error <5 ppm), (ii) characteristic MS/MS fragmentation patterns, and (iii) chromatographic retention time.

biodefluorinated.[34] These data infer the TP256 structure as $C_6H_2F_8O_2$ and suggest that reductive defluorination might occur at the α-C of PFMeUPA($C_6HF_9O_2$, Figure S6) via hydrogenolysis and HF elimination. These fragments show the evidence of a single substituted C−F bond (C_5HF_8 fragment) and a saturated branched perfluorinated fragment C_5F_7 (−HF from C_5HF_8 fragment and the complete branch of the saturated part of the PFMeUPA fragment). The formation of TP256 was accompanied by significant fluoride ion release, resulting in 14−19% (Figure 1F) of the maximum theoretical defluorination of PFMeUPA, indicative of the replacement of at least 1 out of 9 fluorine atoms (~11%).

Another intermediate (TP276) was likely produced by the addition of two hydrogen atoms at the unsaturated carbon double bond (Figure S8), and TP259 was produced by further replacing one fluorine with hydrogen (Figure S9). This suggests that the hydrogenation of PFMeUPA was initiated at the C=C bond. In summary, the TP profiles (Figures S7 and S9) revealed one defluorination product and two hydrogenation products. The same transformation products were also reported in the anaerobic defluorinating consortium KB1, potentially indicating the crucial role (and susceptibility) of unsaturated carbon bonds in C−F cleavage.[31]

We further monitored the temporal formation trends of TPs in the methanol-amended group at days 19, 34, 46, 53, 71, and 89. As shown in Figure S10, TP256 reached its maximum concentration on day 46, followed by a progressive decline. Concomitantly, TP259 began accumulating at this point, while TP276 exhibited continuous accumulation throughout the incubation period. Based on these dynamics, we postulate the PFMeUPA degradation pathway as follows (Figure 2): (a) Initial reductive defluorination occurs at the C−F bond adjacent to the C=C bond, providing an enzyme binding site that leads to the formation of TP256, the major contributor to fluoride ion release; (b) Hydrogenation of the unsaturated C=C bond proceeds concurrently, yielding the saturated terminal product TP276; (c) Secondary hydrogenation of TP256 forms the saturated polyfluorinated product TP259.

3.3. Microbial Community Adaptation to PFMeUP after 80 Days of Enrichment. After 80 days of incubation, when no further fluoride release was detected, samples from the initial inoculum (O), experimental groups M, F, A, and L, and control groups NS (no_substrate) and FNF (formate with no PFAS) were collected for 16S rRNA gene sequencing. Although the substrates (methanol, formate, acetate, and lactate) elicit distinct microbial activities, all consortia consistently achieved the reductive defluorination of PFMeUPA. This functional convergence motivated our analytical focus on shared microbial taxa across treatment groups. A significant shift in the microbial community was observed in the PFMeUPA-amended groups compared with the initial inoculum (O). The most abundant phyla in groups M, F, A, and L were *Bacteroidota* and *Firmicutes*, which accounted for 50.2 to 68.1%, and remained relatively stable during incubation[67] (Figure S11). However, the relative abundances of *Campylobacterota, Chloroflexi, Desulfobacterota, Proteobacteria, Euryarchaeota, and Halobacterota* increased notably from 0.02, 7.5, 1.2, 2.5, 0.62, and 0.01% in the initial inoculum to 18.5% (A), 20.9% (M), 25.4% (L), 8.8% (F), 43.1% (FNF), and 24.1% (NS), respectively. Incidentally, an enrichment of *Chloroflexi* was similarly observed in a dehalogenation consortium after 10-month incubation with 10 mg/L trifluoroacetate (TFA) and 5 mg/L PFOA.[28,68]

Variations in the microbial community composition and relative abundance at the genus level were analyzed to provide further insights into the microorganisms involved in defluorination (Figure 3). After 80 days of incubation, 13 different genera (*Sulfurospirillum, Romboutsia, Petrimonas, Macellibacteroides, JGI-0000079-D21, Geofilum, Fastidiosipila, Ercella, Desulfomicrobium, Clostridium sensu stricto 1, Candidatus Caldatribacterium, Blvii28 wastewater-sludge group*, and *Asaccharospora*) increased in groups M, A, F, and L compared to

https://doi.org/10.1021/acs.est.5c06744
Environ. Sci. Technol. 2025, 59, 21567−21578

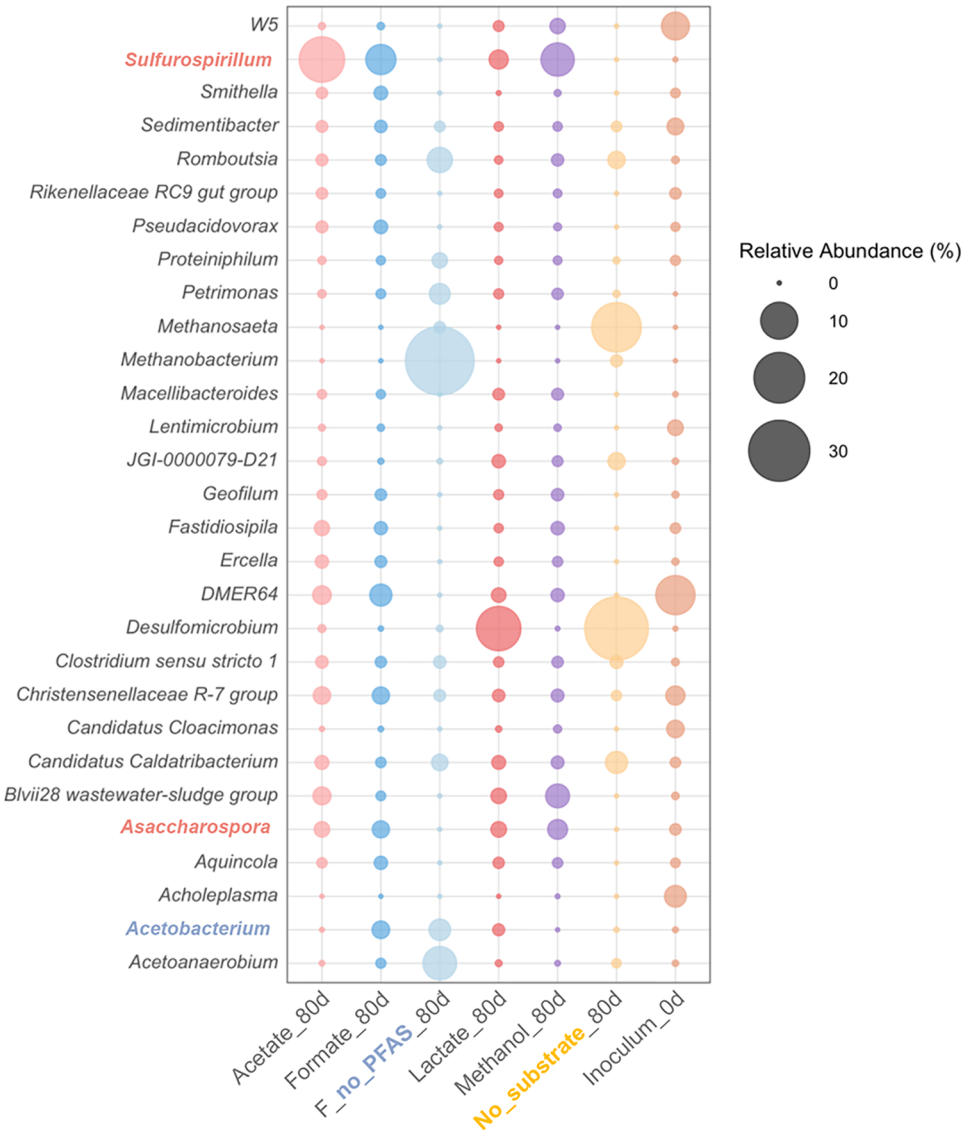

Figure 3. Bubble plot showing genus-level microbial community composition after 80-day incubation across treatment groups: (1) acetate + PFMeUPA, (2) formate + PFMeUPA, (3) lactate + PFMeUPA, (4) methanol + PFMeUPA, (5) no substrate control, (6) formate without PFAS control, and (7) inoculum. Each column represents a treatment group, with bubble size indicating relative abundance, and color representing taxonomic classification. The plot displays the 30 most abundant genera, revealing substrate-dependent community restructuring under different PFMeUPA degradation conditions.

the inoculum. Strikingly, genera *including Romboutsia, Methanobacterium*, *C. Caldatribacterium*, and *Acetoanaerobium* exhibited reduced abundance in PFMeUPA-amended group F compared to substrate-matched control (F_no_PFAS), indicating specific sensitivity to PFMeUPA exposure. *Acetobacterium* was exclusively detected in groups F and L at relative abundances of 1.6, 1.7, and 1.3%, possibly due to their obligate dependence on hydrogen produced through hydrogenase-catalyzed oxidation of formate and lactate.[69] This observation aligns with previous reports that *Acetobacterium* species possessing both fluoride exporters and caffeate reductases could mediate reductive defluorination of PFMeUPA coupled with hydrogenation.[34] However, the defluorination mechanisms in groups M and A (where *Acetobacterium* was undetectable) require further investigation to explore alternative PFMeUPA degradation pathways.

The genera *Sulfurospirillum* and *Asaccharospora* were significantly enriched across all treated groups (with relative abundance increasing from <0.01 to 2−16%) but not in the no substrate (NS) and no PFAS (FNF) controls. Thus, *Sulfurospirillum* preferentially proliferated when both PFMeUPA and either of these carbon sources were added (Figure 3). Several newly isolated strains of *Sulfurospirillum* have demonstrated the ability to dechlorinate tetrachloroethene, suggesting their potential dehalogenation (i.e., defluorination) capacity.[70,71]

3.4. Fluoride Exporter Search Revealed Potential Defluorination Candidates. To further discern the microbial defluorination organisms and pathways, metagenomic sequencing was conducted on 5 different samples (inoculum, methanol, formate, acetate, and lactate). From the four treatments and original inoculum, we recovered 256 metagenome-assembled genomes (MAGs) of medium to high quality (<10% contamination and >50% completeness). These filtered MAGs were then annotated using the KEGG, PFAM, and NCBI databases. As low levels of fluoride derived

https://doi.org/10.1021/acs.est.5c06744
Environ. Sci. Technol. 2025, 59, 21567−21578

Table 1. Relative Abundance of Metagenome-Assembled Genomes (MAGs)[a]

Genomes	Delta_M_O (%)	Delta_L_O (%)	Delta_F_O (%)	Delta_A_O (%)
A_bin.66	0.000	0.000	0.040	0.118
A_bin.69	0.273	0.362	0.087	0.271
co_bin.100	0.029	-0.099	0.020	0.041
co_bin.103	-0.083	-0.089	-0.056	-0.078
co_bin.105	0.017	-0.019	-0.016	-0.024
co_bin.116	0.046	0.020	0.036	0.036
co_bin.117	0.231	0.124	0.227	0.213
co_bin.121	0.012	-0.001	0.058	0.012
co_bin.122	0.154	-0.064	-0.015	-0.037
co_bin.124	0.008	0.000	0.116	0.027
co_bin.13	0.031	0.026	0.054	0.094
co_bin.133	0.005	-0.002	0.027	0.006
co_bin.145	-0.002	-0.006	0.011	0.012
co_bin.153	-0.102	-0.103	-0.098	-0.097
co_bin.154	0.022	0.015	0.077	0.031
co_bin.170	0.083	0.036	0.103	0.062
co_bin.173	0.007	0.051	-0.003	0.139
co_bin.180	0.010	0.054	0.001	0.004
co_bin.20	0.005	0.064	0.073	0.138
co_bin.204	0.052	0.030	0.020	0.041
co_bin.207	0.050	0.031	0.055	0.056
co_bin.209	-0.613	-0.622	-0.604	-0.619
co_bin.227	0.012	0.002	0.036	0.010
co_bin.233	0.486	0.156	0.282	0.161
co_bin.235	-0.003	-0.007	0.100	0.019
co_bin.237	0.040	0.035	0.084	0.084
co_bin.240	-0.004	-0.008	0.002	0.009
co_bin.246	0.040	0.004	0.053	0.075
co_bin.27	0.000	-0.010	0.037	0.020
co_bin.3	-0.196	-0.198	-0.199	-0.197
co_bin.34	0.040	0.021	0.053	0.062
co_bin.37	-0.001	-0.010	-0.005	-0.007
co_bin.39	0.050	0.045	0.169	0.130
co_bin.41	0.011	0.019	0.084	0.030
co_bin.45	0.006	0.002	0.014	0.013
co_bin.6	0.024	0.016	0.033	0.031
co_bin.65	-0.046	-0.035	-0.038	-0.047
co_bin.75	0.056	0.030	0.025	0.109
co_bin.86	0.016	0.013	0.047	0.024
F_bin.15	0.017	0.018	0.099	0.005
F_bin.38	0.095	-0.118	0.042	-0.124
L_bin.1	0.000	0.262	0.103	0.000
L_bin.19	0.000	0.164	0.039	0.000
L_bin.24	0.000	0.450	0.000	0.074
L_bin.5	0.000	0.157	0.000	0.000
M_bin.36	0.160	0.000	0.003	0.002
M_bin.38	1.154	0.000	0.000	0.000
M_bin.39	0.636	0.000	0.000	0.000
M_bin.41	0.518	0.000	0.000	0.000
M_bin.68	1.136	0.268	0.425	0.770
O_bin.29	-0.388	-0.388	-0.388	-0.388
O_bin.33	-0.295	-0.304	-0.287	-0.278

[a]Annotated *crcB* genes exhibited substrate-dependent enrichment relative to the initial inoculum. Blue and red bars, respectively, indicate increased and decreased relative abundance in experimental groups compared with the inoculum. The taxonomy of genomes is detailed in Table S3.

from defluorination can inhibit essential enzymes,[72−74] microorganisms that can defluorinate PFMeUPA must encode transporters to actively export intracellular fluoride. Thus, we searched all the MAGs for the fluoride exporter gene (*crcB*) and found it in 52 genomes (Table 1). The structure of the representative *crcB* in A_bin.69 was predicted to form a homodimer using[75] (Figure S12; AlphaFold3;[76] ipTM = 99.98, pTM = 99.975), which is highly similar to the experimentally resolved reference (PDB: Q7VYU0; TM-score = 0.977).[77,78] By confirming the sequence and structural identity of Fluc proteins, we deduced that the identified *crcB* in our reconstructed MAGs may export intracellular fluoride ions to facilitate the microbial defluorination process.

To further identify the reductive defluorination enzymes, a previous study reported that an electron-bifurcating caffeate reductase complex (CarCDE) could specifically catalyze

https://doi.org/10.1021/acs.est.5c06744
Environ. Sci. Technol. 2025, 59, 21567−21578

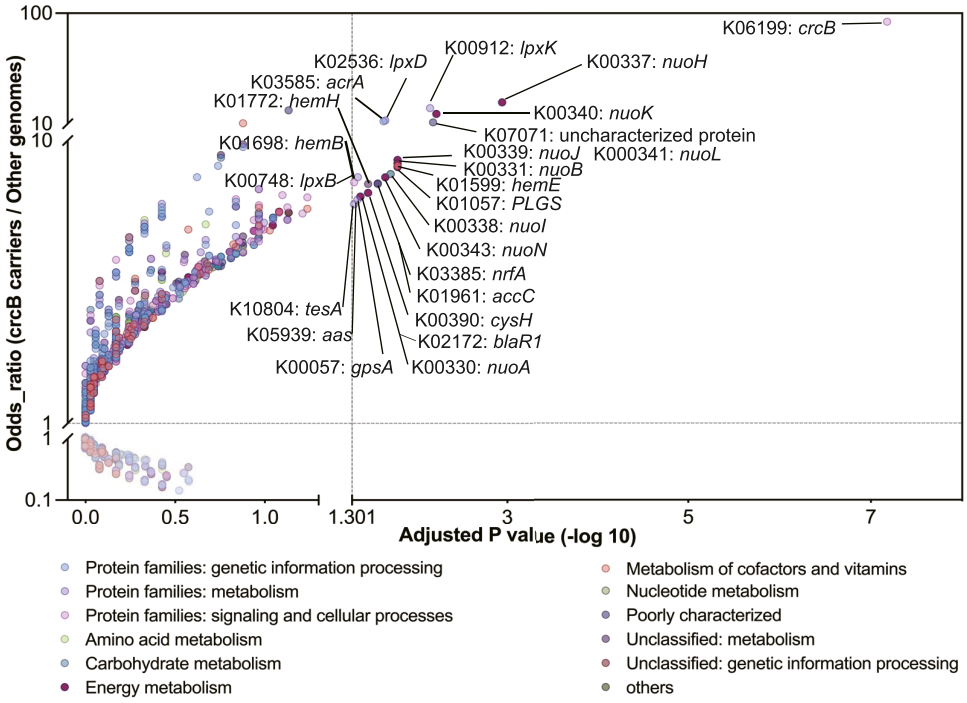

Figure 4. Functional enrichment analysis of fluoride exporter-containing genomes versus noncarrier genomes. The *x*-axis represents the statistical significance [$-\log_{10}$(FDR-adjusted p-value)], with a vertical dashed line marking the significance threshold (1.301, FDR = 0.05). The *y*-axis indicates the $\log_2$-transformed odds ratio fold change, where values above 1 denote functional enrichment in exporter-containing genomes. Semitransparent markers correspond to KEGG Orthology (KO) terms lacking statistical significance (FDR ≥ 0.05), while colored points reflect their respective metabolic categories according to KEGG classification.

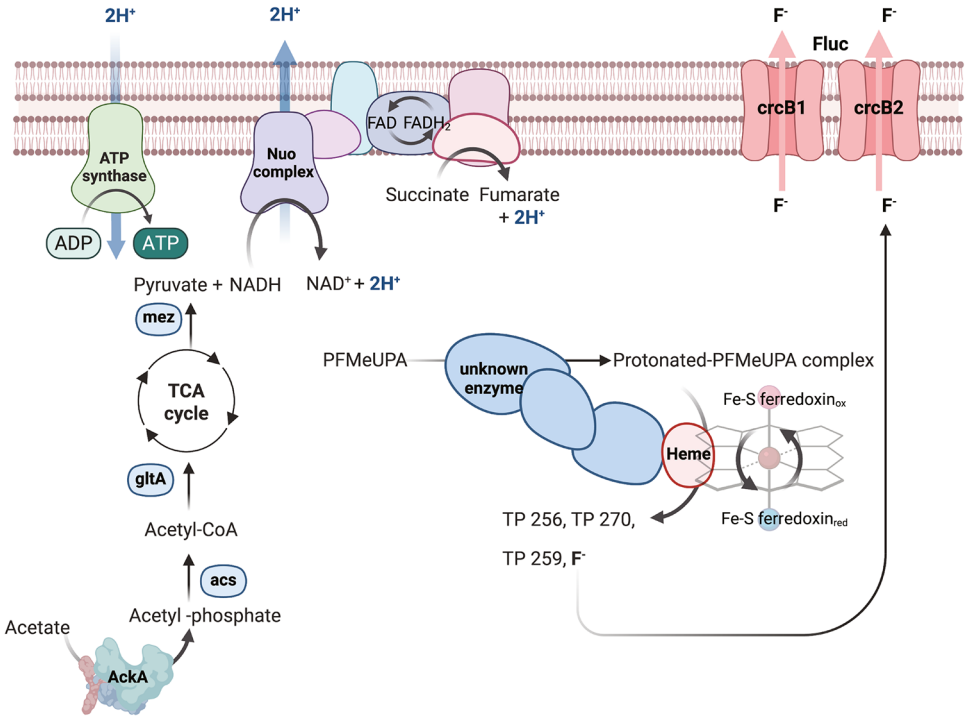

Figure 5. Reconstructed putative metabolic networks in candidate defluorinating genomes M_bin.68 (classified as *Sulfurospirillum sp001548035*) and A_bin.69 (identified as *Sulfurospirillum cavolei*), based on: (i) substrate utilization potential (using acetate amendment as an example), (ii) gene enrichment analysis, and (iii) key enzymatic functions. Annotated pathways include acetate metabolism (AckA: acetate kinase), electron transport (Nuo complex: NADH-quinone oxidoreductase), flavin-mediated redox reactions (FAD/$FADH_2$ oxidized/reduced flavin adenine dinucleotide), cofactor (Heme: ferrochelatase), and fluoride detoxification system (*crcB*: fluoride exporter).

unsaturated carbon−carbon bonds.[34] Through integrated Pfam HMM and KEGG Orthology screening of annotated genomes, we identified key electron-bifurcating enzymes—including caffeate reductase (CarCDE; EC 1.3.1.108), hydrogenases

https://doi.org/10.1021/acs.est.5c06744
Environ. Sci. Technol. 2025, 59, 21567−21578

(HydABCDE/Hyt; EC 1.12.1.4, 1.12.1.3, 1.17.1.11), and transhydrogenases (Ldh; EC 1.6.1.4), among which the CarCDE cluster, a putative defluorination catalyst, was detected in three genomes: co_bin.210, co_bin.165, and L_bin.19. Crucially, only *Acetobacterium* (L_bin.19), a validated defluorinating genus, coencoded the fluoride efflux gene *crcB*. Concurrently detected bifurcating enzymes in formate/hydrogen/lactate dehydrogenase pathways may modulate redox conditions, but they are unlikely to directly drive reductive defluorination.

Of 52 MAGs encoding *crcB* genes, 23 demonstrated increased abundances after incubation with PFMeUPA (Table 1, in blue), suggesting that they might contribute to and benefit from PFMeUPA degradation. Thus, we performed gene enrichment analysis between them (n = 23) and others (n = 233) to uncover potential defluorination-associated genes. Twenty-eight KEGG Orthology (KO) groups were significantly enriched in the positive group (Figure 4; Fisher test: Padj <0.05, odds ratio >1), including a series of *nuo* genes together encoding NADH: quinone oxidoreductase (Nuo complex, Type I NADH dehydrogenase).[79] The Nuo complex catalyzes NADH oxidation coupled to menaquinone reduction and transfers electrons via FMN and iron−sulfur (Fe−S) clusters.[80] NADH could probably provide protons and a reductive force for the defluorination process based on the enzyme reaction. K01772 (adjusted P = 0.016, odds ratio = 1.80) encodes a membrane-associated ferrochelatase (EC 4.99.1.1), the metalloenzyme that catalyzes the terminal reaction of heme biosynthesis through Fe^{2+} insertion into protoporphyrin IX to form protoheme. This protein features a conserved histidine-rich active site loop that enables reactions with various redox potential requirements to take place.[81] Other significantly enriched genes were primarily associated with substrate assimilation pathways and likely did not directly contribute to the biodefluorination activity.

In summary, groups F and L, which contained the known defluorinating bacterium *Acetobacterium*, exhibited a putative defluorination pathway involving C−F bond cleavage at unsaturated carbon sites. Genomic evidence from *Acetobacterium* strain L_bin.19 (GTDB taxonomy) identified two key genetic elements facilitating this process: (1) caffeate reduction bifurcating protein-the car operon, which may initiate attack at double-bonded carbons, and (2) *crcB*-encoded fluoride exporters that mitigate intracellular fluoride toxicity.[34]

For groups M and A, which lacked detectable *Acetobacterium*, the 23 positive-group genomes were systematically screened through three complementary approaches: (i) gene enrichment analysis, (ii) identification of anaerobic methane/acetate metabolism markers (KOs), and (iii) functional annotation of putative defluorination enzymes. Only two genomes met all criteria, M_bin.68 (classified as *Sulfurospirillum sp001548035*) and A_bin.69 (identified as *Sulfurospirillum cavolei*), suggesting these sulfur-reducing bacteria may employ distinct defluorination mechanisms.

3.5. Proposed Metabolic Pathway for PFAS Defluorination. Based on the meta-omics analysis, here we propose the metabolic pathway for PFAS defluorination in a mixed culture (group A), featuring *Sulfurospirillum* (M_bin.68 and A_bin.69) as shown in Figure 5. The anaerobic defluorination pathway is initiated through acetate kinase [EC:2.7.2.1] to generate ATP. Electrons are transferred through soluble carriers (e.g., quinones) to the membrane-bound Nuo complex, yielding NADH ($E^{\circ\prime}$ = −320 mV) as the key reductant. PFMeUPA activation begins with an (unknown) enzyme-mediated C−C bond scission at the α-β unsaturated carbon (C═C), followed by NADH-dependent hydride transfer to the α-carbon to form hydrogenated PFMeUPA. Subsequent defluorination is facilitated by a heme−Fe-S center that orchestrates acid−base catalysis—first abstracting protons from C_3 via ferredoxin, then enabling β-elimination of F^- from C_2 to produce TP256 and free fluoride, which was further exported by the transmembrane *crcB* system. The Nuo-ferredoxin system could maintain the required ←400 mV potential for C−F bond cleavage. A similar pathway happened to form TP259 and TP276 without the β-elimination of F^-.

Environmental Implications. This study demonstrates that anaerobic microbial reductive defluorination of a C_6 perfluorinated compound can be accomplished by common municipal anaerobic digestion sludge and enhanced through amendment with common substrates such as methanol, formate, acetate, or lactate. Structural analysis reveals preferential bioavailability at unsaturated moieties, where initial C−F bond cleavage occurs at sp^2-hybridized carbons—a critical first step in breaking down these persistent contaminants. This suggests some key applicability scenarios: (1) degradation of tert-unsaturated PFAIs (e.g., 6:2 FTAB) in fire-training ground leachates, where the β-unsaturated ketone group enhances susceptibility to anaerobic hydrogenolysis. Treatment of electrochemical fluorination-derived wastes containing unsaturated byproducts (e.g., PFCAs = C−C, such as $F(CF_2)_4CH$ = CHCOOH); (2) co-degradation of chlorinated solvents (e.g., TCE) and unsaturated PFAS in groundwater plumes; and (3) Integration into WWTP anaerobic digesters to target unsaturated PFAS (e.g., isobranched PFPAs with vinylogous structures) concentrated in sludge.

The resulting polyfluorinated intermediates may undergo further defluorination by environmental microbial communities, enabling more complete degradation cascades. However, successful defluorination requires microbial tolerance to fluoride toxicity, necessitating genetic adaptations such as crcB-encoded fluoride exporters. Through comparative genomic analysis of *crcB*-containing versus non-*crcB* genomes and abundance changes, we identified two novel *Sulfurospirillum* species as promising defluorinating candidates, potentially employing a distinct Nuo-ferredoxin enzymatic system. We recognize that the presence of *crcB* does not guarantee PFAS defluorination capabilities, but our results indicate that it can be a useful biomarker to discover putative defluorinating species. Future validation using axenic cultures of these isolates will be essential to confirm their metabolic capabilities and characterize the step-by-step genes in the proposed defluorination pathway.

The discovery of these organisms not only expands the known diversity of potential defluorinating bacteria but also demonstrates the untapped potential of anaerobic municipal sludge for PFAS remediation, offering a sustainable alternative to energy-intensive physical/chemical treatment methods. Importantly, we focused on PFAS degradation by indigenous bacteria in anaerobic digestion sludge and established a framework that enables the stepwise identification of functional microorganisms and associated mechanisms directly from complex microbial communities.

https://doi.org/10.1021/acs.est.5c06744
Environ. Sci. Technol. 2025, 59, 21567−21578

■ ASSOCIATED CONTENT

Supporting Information

The Supporting Information is available free of charge at https://pubs.acs.org/doi/10.1021/acs.est.5c06744.

Additional experimental details, materials, and methods; parent compound removal and fluoride ion formation in abiotic controls and hydrogen-amended groups; substrate and methane concentration in treated groups; LC-QTOFMS/MS chromatographs and full-scan and MS2 spectra of TPs; temporal TP analysis; microbial community shifts; properties of recovered MAGs; detailed information on KOs from Fisher-test results; fluoride exporter protein structure alignment (PDF)

■ AUTHOR INFORMATION

Corresponding Author

He-Ping Zhao − *State Key Laboratory of Soil Pollution Control and Safety, Zhejiang University, Hangzhou 310058, China; MOE Key Lab of Environmental Remediation and Ecosystem Health, College of Environmental and Resource Science, Zhejiang University, Hangzhou 310058, China;* orcid.org/0000-0002-5177-8010; Email: zhaohp@zju.edu.cn

Authors

Qiu-Jin Xu − *State Key Laboratory of Soil Pollution Control and Safety, Zhejiang University, Hangzhou 310058, China; MOE Key Lab of Environmental Remediation and Ecosystem Health, College of Environmental and Resource Science, Zhejiang University, Hangzhou 310058, China;* orcid.org/0000-0001-9278-8357

Carolyn R. Cornell − *Department of Civil and Environmental Engineering and Rice WaTER Institute, Rice University, Houston, Texas 77005, United States;* orcid.org/0000-0001-5355-3248

Chuncheng Wu − *Department of Civil and Environmental Engineering and Rice WaTER Institute, Rice University, Houston, Texas 77005, United States*

Sarah Glass − *Department of Civil and Environmental Engineering and Rice WaTER Institute, Rice University, Houston, Texas 77005, United States*

Jacques Mathieu − *Department of Civil and Environmental Engineering and Rice WaTER Institute, Rice University, Houston, Texas 77005, United States;* orcid.org/0000-0003-1776-8772

Pedro J. J. Alvarez − *Department of Civil and Environmental Engineering and Rice WaTER Institute, Rice University, Houston, Texas 77005, United States;* orcid.org/0000-0002-6725-7199

Complete contact information is available at: https://pubs.acs.org/10.1021/acs.est.5c06744

Notes

The authors declare no competing financial interest.

■ ACKNOWLEDGMENTS

The authors greatly thank the "National Natural Science Foundation of China (Grant Nos. 22325604)", the "Key Research & Development Program of Zhejiang Province (2025C02214)" for their financial support. PJA was funded by the Rice WaTER Institute. The authors would like to thank the Shared Equipment Authority of Rice University for the help with HPLC, LC QQQ/MS, LC QTOF/MS, and F-HMR analysis.

■ REFERENCES

(1) Glüge, J.; Scheringer, M.; Cousins, I. T.; DeWitt, J. C.; Goldenman, G.; Herzke, D.; Lohmann, R.; Ng, C. A.; Trier, X.; Wang, Z. An Overview of the Uses of Per- and Polyfluoroalkyl Substances (PFAS). *Environ. Sci. Process. Impacts* **2020**, *22* (12), 2345−2373.

(2) Wang, Z.; DeWitt, J. C.; Higgins, C. P.; Cousins, I. T. A Never-Ending Story of Per- and Polyfluoroalkyl Substances (PFASs)? *Environ. Sci. Technol.* **2017**, *51* (5), 2508−2518.

(3) Evich, M. G.; Davis, M. J. B.; McCord, J. P.; Acrey, B.; Awkerman, J. A.; Knappe, D. R. U.; Lindstrom, A. B.; Speth, T. F.; Tebes-Stevens, C.; Strynar, M. J.; Wang, Z.; Weber, E. J.; Henderson, W. M.; Washington, J. W. Per- and Polyfluoroalkyl Substances in the Environment. *Science* **2022**, *375* (6580), No. eabg9065.

(4) Nielsen, F.; Fischer, F. C.; Leth, P. M.; Grandjean, P. Occurrence of Major Perfluorinated Alkylate Substances in Human Blood and Target Organs. *Environ. Sci. Technol.* **2024**, *58*, 143−149.

(5) Grunfeld, D. A.; Gilbert, D.; Hou, J.; Jones, A. M.; Lee, M. J.; Kibbey, T. C. G.; O'Carroll, D. M. Underestimated Burden of Per- and Polyfluoroalkyl Substances in Global Surface Waters and Groundwaters. *Nat. Geosci.* **2024**, *17* (4), 340−346.

(6) EU Regulations for PFAS. https://eur-lex.europa.eu/legal-content/EN/TXT/HTML/?uri=CELEX:32020L2184#d1e32-49-1. accessed 2020−12−16.

(7) EPA PFAS Regulation. https://www.federalregister.gov/d/2024-07773. accessed 2024−4-26.

(8) Yang, L.; Chen, Z.; Goult, C. A.; Schlatzer, T.; Paton, R. S.; Gouverneur, V. Phosphate-Enabled Mechanochemical PFAS Destruction for Fluoride Reuse. *Nature* **2025**, *640* (8057), 100−106.

(9) Wang, N.; Lv, H.; Zhou, Y.; Zhu, L.; Hu, Y.; Majima, T.; Tang, H. Complete Defluorination and Mineralization of Perfluorooctanoic Acid by a Mechanochemical Method Using Alumina and Persulfate. *Environ. Sci. Technol.* **2019**, *53* (14), 8302−8313.

(10) Duan, L.; Gu, M.; Wang, M.; Liu, L.; Cheng, X.; Fan, X.; Huang, J. Mechanochemical Destruction of Perfluorooctane Sulfonate (PFOS) Using Boron Carbide (B4C). *J. Hazard. Mater.* **2025**, *486*, No. 137044.

(11) Hao, S.; Choi, Y.-J.; Wu, B.; Higgins, C. P.; Deeb, R.; Strathmann, T. J. Hydrothermal Alkaline Treatment for Destruction of Per- and Polyfluoroalkyl Substances in Aqueous Film-Forming Foam. *Environ. Sci. Technol.* **2021**, *55* (5), 3283−3295.

(12) Wu, B.; Hao, S.; Choi, Y.; Higgins, C. P.; Deeb, R.; Strathmann, T. J. Rapid Destruction and Defluorination of Perfluorooctanesulfonate by Alkaline Hydrothermal Reaction. *Environ. Sci. Technol. Lett.* **2019**, *6* (10), 630−636.

(13) Xu, M.-G.; Huang, C.; Zhao, L.; Rappé, A. K.; Kennedy, E. M.; Stockenhuber, M.; Mackie, J. C.; Weber, N. H.; Lucas, J. A.; Ahmed, M.; Blotevogel, J.; Lu, W. Direct Measurement of Fluorocarbon Radicals in the Thermal Destruction of Perfluorohexanoic Acid Using Photoionization Mass Spectrometry. *Sci. Adv.* **2025**, *11* (9), No. eadt3363.

(14) Sun, R.; Alinezhad, A.; Altarawneh, M.; Ateia, M.; Blotevogel, J.; Mai, J.; Naidu, R.; Pignatello, J.; Rappe, A.; Zhang, X.; Xiao, F. New Insights into Thermal Degradation Products of Long-Chain Per- and Polyfluoroalkyl Substances (PFAS) and Their Mineralization Enhancement Using Additives. *Environ. Sci. Technol.* **2024**, *58* (50), 22417−22430.

(15) Gao, J.; Liu, Z.; Chen, Z.; Rao, D.; Che, S.; Gu, C.; Men, Y.; Huang, J.; Liu, J. Photochemical Degradation Pathways and Near-Complete Defluorination of Chlorinated Polyfluoroalkyl Substances. *Nat. Water* **2023**, *1* (4), 381−390.

(16) Wang, Z.; Jin, X.; Hong, R.; Wang, X.; Chen, Z.; Gao, G.; He, H.; Liu, J.; Gu, C. New Indole Derivative Heterogeneous System for the Synergistic Reduction and Oxidation of Various Per-/Polyfluoroalkyl Substances: Insights into the Degradation/Defluorination Mechanism. *Environ. Sci. Technol.* **2023**, *57* (50), 21459−21469.

(17) Guan, Y.; Liu, Z.; Yang, N.; Yang, S.; Quispe-Cardenas, L. E.; Liu, J.; Yang, Y. Near-Complete Destruction of PFAS in Aqueous Film-Forming Foam by Integrated Photo-Electrochemical Processes. *Nat. Water* **2024**, *2* (5), 443−452.
(18) Cheng, Y.; Deng, B.; Scotland, P.; Eddy, L.; Hassan, A.; Wang, B.; Silva, K. J.; Li, B.; Wyss, K. M.; Ucak-Astarlioglu, M. G.; Chen, J.; Liu, Q.; Si, T.; Xu, S.; Gao, X.; JeBailey, K.; Jana, D.; Torres, M. A.; Wong, M. S.; Yakobson, B. I.; Griggs, C.; McCary, M. A.; Zhao, Y.; Tour, J. M. Electrothermal Mineralization of Per- and Polyfluoroalkyl Substances for Soil Remediation. *Nat. Commun.* **2024**, *15* (1), No. 6117.
(19) Yin, S.; López, J. F.; Sandoval-Pauker, C.; Calvillo Solís, J. J.; Glass, S.; Habib, A.; Lee, W.-Y.; Wong, M. S.; Alvarez, P. J. J.; Villagrán, D. Trap-n-Zap: Electrocatalytic Degradation of Perfluorooctanoic Acid (PFOA) with UiO-66 Modified Boron Nitride Electrodes at Environmentally Relevant Concentrations. *Appl. Catal., B* **2024**, *355*, No. 124136.
(20) Solís, J. J. C.; Sandoval-Pauker, C.; Bai, D.; Yin, S.; Senftle, T. P.; Villagrán, D. Electrochemical Reduction of Perfluorooctanoic Acid (PFOA): An Experimental and Theoretical Approach. *J. Am. Chem. Soc.* **2024**, *146* (15), 10687−10698.
(21) Key, B. D.; Howell, R. D.; Criddle, C. S. Defluorination of Organofluorine Sulfur Compounds by *Pseudomonas* Sp. Strain D2. *Environ. Sci. Technol.* **1998**, *32* (15), 2283−2287.
(22) Marchetto, F.; Roverso, M.; Righetti, D.; Bogialli, S.; Filippini, F.; Bergantino, E.; Sforza, E. Bioremediation of Per- and Poly-Fluoroalkyl Substances (PFAS) by Synechocystis Sp. PCC 6803: A Chassis for a Synthetic Biology Approach. *Life* **2021**, *11* (12), No. 1300.
(23) Ochoa-Herrera, V.; Field, J. A.; Luna-Velasco, A.; Sierra-Alvarez, R. Microbial Toxicity and Biodegradability of Perfluorooctane Sulfonate (PFOS) and Shorter Chain Perfluoroalkyl and Polyfluoroalkyl Substances (PFASs). *Environ. Sci. Process. Impacts* **2016**, *18* (9), 1236−1246.
(24) Huang, S.; Jaffé, P. R. Defluorination of Perfluorooctanoic Acid (PFOA) and Perfluorooctane Sulfonate (PFOS) by *Acidimicrobium* Sp. Strain A6. *Environ. Sci. Technol.* **2019**, *53* (19), 11410−11419.
(25) Huang, S.; Sima, M.; Long, Y.; Messenger, C.; Jaffé, P. R. Anaerobic Degradation of Perfluorooctanoic Acid (PFOA) in Biosolids by Acidimicrobium Sp. Strain A6. *J. Hazard. Mater.* **2022**, *424*, No. 127699.
(26) Park, J.; Huang, S.; Koel, B. E.; Jaffé, P. R. Enhanced Feammox Activity and Perfluorooctanoic Acid (PFOA) Degradation by Acidimicrobium Sp. Strain A6 Using PAA-Coated Ferrihydrite as an Electron Acceptor. *J. Hazard. Mater.* **2023**, *459*, No. 132039.
(27) Ruiz-Urigüen, M.; Shuai, W.; Huang, S.; Jaffé, P. R. Biodegradation of PFOA in Microbial Electrolysis Cells by Acidimicrobiaceae Sp. Strain A6. *Chemosphere* **2022**, *292*, No. 133506.
(28) Tang, Z.; Vogel, T. M.; Wang, Q.; Wei, C.; Ali, M.; Song, X. Microbial Defluorination of TFA, PFOA, and HFPO-DA by a Native Microbial Consortium under Anoxic Conditions. *J. Hazard. Mater.* **2024**, *465*, No. 133217.
(29) Lorah, M. M.; He, K.; Blaney, L.; Akob, D. M.; Harris, C.; Tokranov, A.; Hopkins, Z.; Shedd, B. P. Anaerobic Biodegradation of Perfluorooctane Sulfonate (PFOS) and Microbial Community Composition in Soil Amended with a Dechlorinating Culture and Chlorinated Solvents. *Sci. Total Environ.* **2024**, *932*, No. 172996.
(30) Liu, J.; Edwards, E.; Van Hamme, J.; Manefield, M.; Higgins, C. P.; Blotevogel, J.; Liu, J.; Lee, L. S. Correspondence on "Defluorination of Perfluorooctanoic Acid (PFOA) and Perfluorooctane Sulfonate (PFOS) by *Acidimicrobium* Sp. Strain A6.". *Environ. Sci. Technol.* **2023**, *57* (48), 20440−20442.
(31) Bentel, M. J.; Yu, Y.; Xu, L.; Li, Z.; Wong, B. M.; Men, Y.; Liu, J. Defluorination of Per- and Polyfluoroalkyl Substances (PFASs) with Hydrated Electrons: Structural Dependence and Implications to PFAS Remediation and Management. *Environ. Sci. Technol.* **2019**, *53* (7), 3718−3728.
(32) Yu, Y.; Zhang, K.; Li, Z.; Ren, C.; Chen, J.; Lin, Y.-H.; Liu, J.; Men, Y. Microbial Cleavage of C−F Bonds in Two C_6 Per- and Polyfluorinated Compounds via Reductive Defluorination. *Environ. Sci. Technol.* **2020**, *54* (22), 14393−14402.
(33) Jin, B.; Zhu, Y.; Zhao, W.; Liu, Z.; Che, S.; Chen, K.; Lin, Y.-H.; Liu, J.; Men, Y. Aerobic Biotransformation and Defluorination of Fluoroalkylether Substances (Ether PFAS): Substrate Specificity, Pathways, and Applications. *Environ. Sci. Technol. Lett.* **2023**, *10* (9), 755−761.
(34) Yu, Y.; Xu, F.; Zhao, W.; Thoma, C.; Che, S.; Richman, J. E.; Jin, B.; Zhu, Y.; Xing, Y.; Wackett, L.; Men, Y. Electron Bifurcation and Fluoride Efflux Systems Implicated in Defluorination of Perfluorinated Unsaturated Carboxylic Acids by *Acetobacterium* Spp. *Sci. Adv.* **2024**, *10* (29), No. eado2957.
(35) Kim, J.; Xin, X.; Hawkins, G. L.; Huang, Q.; Huang, C.-H. Occurrence, Fate, and Removal of Per- and Polyfluoroalkyl Substances (PFAS) in Small- and Large-Scale Municipal Wastewater Treatment Facilities in the United States. *ACS EST Water* **2024**, *4* (12), 5428−5436.
(36) Lenka, S. P.; Kah, M.; Padhye, L. P. A Review of the Occurrence, Transformation, and Removal of Poly- and Perfluoroalkyl Substances (PFAS) in Wastewater Treatment Plants. *Water Res.* **2021**, *199*, No. 117187.
(37) Skinner, J. P.; Raderstorf, A.; Rittmann, B. E.; Delgado, A. G. Biotransforming the "Forever Chemicals": Trends and Insights from Microbiological Studies on PFAS. *Environ. Sci. Technol.* **2025**, *59*, 5417−5430.
(38) Oviedo-Vargas, D.; Anton, J.; Coleman-Kammula, S.; Qin, X. Quantification of PFAS in Soils Treated with Biosolids in Ten Northeastern US Farms. *Sci. Rep.* **2025**, *15* (1), No. 5582.
(39) Ouyang, W.-Y.; Birkigt, J.; Richnow, H. H.; Adrian, L. Anaerobic Transformation and Detoxification of Sulfamethoxazole by Sulfate-Reducing Enrichments and *Desulfovibrio Vulgaris*. *Environ. Sci. Technol.* **2021**, *55* (1), 271−282.
(40) Shrestha, S.; Xue, S.; Kitt, D.; Song, H.; Truyers, C.; Muermans, M.; Smets, I.; Raskin, L. Anaerobic Dynamic Membrane Bioreactor Development to Facilitate Organic Waste Conversion to Medium-Chain Carboxylic Acids and Their Downstream Recovery. *ACS EST Eng.* **2022**, *2* (2), 169−180.
(41) Stroot, P. Anaerobic Codigestion of Municipal Solid Waste and Biosolids under Various Mixing Conditions—I. Digester Performance. *Water Res.* **2001**, *35* (7), 1804−1816.
(42) Liu, H.; Wang, J.; Wang, A.; Chen, J. Chemical Inhibitors of Methanogenesis and Putative Applications. *Appl. Microbiol. Biotechnol.* **2011**, *89* (5), 1333−1340.
(43) Zorz, J.; Li, C.; Chakraborty, A.; Gittins, D. A.; Surcon, T.; Morrison, N.; Bennett, R.; MacDonald, A.; Hubert, C. R. J. *SituSeq* : An Offline Protocol for Rapid and Remote Nanopore 16S rRNA Amplicon Sequence Analysis. *ISME Commun.* **2023**, *3* (1), No. 33.
(44) Pruesse, E.; Peplies, J.; Glöckner, F. O. SINA: Accurate High-Throughput Multiple Sequence Alignment of Ribosomal RNA Genes. *Bioinformatics* **2012**, *28* (14), 1823−1829.
(45) Quast, C.; Pruesse, E.; Yilmaz, P.; Gerken, J.; Schweer, T.; Yarza, P.; Peplies, J.; Glöckner, F. O. The SILVA Ribosomal RNA Gene Database Project: Improved Data Processing and Web-Based Tools. *Nucleic Acids Res.* **2012**, *41* (D1), D590−D596.
(46) Yilmaz, P.; Parfrey, L. W.; Yarza, P.; Gerken, J.; Pruesse, E.; Quast, C.; Schweer, T.; Peplies, J.; Ludwig, W.; Glöckner, F. O. The SILVA and "All-Species Living Tree Project (LTP)" Taxonomic Frameworks. *Nucleic Acids Res.* **2014**, *42* (D1), D643−D648.
(47) Bolger, A. M.; Lohse, M.; Usadel, B. Trimmomatic: A Flexible Trimmer for Illumina Sequence Data. *Bioinformatics* **2014**, *30* (15), 2114−2120.
(48) Li, D.; Luo, R.; Liu, C.-M.; Leung, C.-M.; Ting, H.-F.; Sadakane, K.; Yamashita, H.; Lam, T.-W. MEGAHIT v1.0: A Fast and Scalable Metagenome Assembler Driven by Advanced Methodologies and Community Practices. *Methods* **2016**, *102*, 3−11.
(49) Kang, D. D.; Li, F.; Kirton, E.; Thomas, A.; Egan, R.; An, H.; Wang, Z. MetaBAT 2: An Adaptive Binning Algorithm for Robust and Efficient Genome Reconstruction from Metagenome Assemblies. *PeerJ* **2019**, *7*, No. e7359.

(50) Parks, D. H.; Imelfort, M.; Skennerton, C. T.; Hugenholtz, P.; Tyson, G. W. CheckM: Assessing the Quality of Microbial Genomes Recovered from Isolates, Single Cells, and Metagenomes. *Genome Res.* **2015**, *25* (7), 1043−1055.
(51) Hyatt, D.; Chen, G.-L.; LoCascio, P. F.; Land, M. L.; Larimer, F. W.; Hauser, L. J. Prodigal: Prokaryotic Gene Recognition and Translation Initiation Site Identification. *BMC Bioinf.* **2010**, *11* (1), No. 119.
(52) Cantalapiedra, C. P.; Hernández-Plaza, A.; Letunic, I.; Bork, P.; Huerta-Cepas, J. eggNOG-Mapper v2: Functional Annotation, Orthology Assignments, and Domain Prediction at the Metagenomic Scale. *Mol. Biol. Evol.* **2021**, *38* (12), 5825−5829.
(53) Eddy, S. R. Accelerated Profile HMM Searches. *PLoS Comput. Biol.* **2011**, *7* (10), No. e1002195.
(54) Buchfink, B.; Reuter, K.; Drost, H.-G. Sensitive Protein Alignments at Tree-of-Life Scale Using DIAMOND. *Nat. Methods* **2021**, *18* (4), 366−368.
(55) Steinegger, M.; Söding, J. MMseqs2 Enables Sensitive Protein Sequence Searching for the Analysis of Massive Data Sets. *Nat. Biotechnol.* **2017**, *35* (11), 1026−1028.
(56) Huerta-Cepas, J.; Szklarczyk, D.; Heller, D.; Hernández-Plaza, A.; Forslund, S. K.; Cook, H.; Mende, D. R.; Letunic, I.; Rattei, T.; Jensen, L. J.; von Mering, C.; Bork, P. eggNOG 5.0: A Hierarchical, Functionally and Phylogenetically Annotated Orthology Resource Based on 5090 Organisms and 2502 Viruses. *Nucleic Acids Res.* **2019**, *47* (D1), D309−D314.
(57) Kanehisa, M.; Sato, Y.; Kawashima, M.; Furumichi, M.; Tanabe, M. KEGG as a Reference Resource for Gene and Protein Annotation. *Nucleic Acids Res.* **2016**, *44* (D1), D457−D462.
(58) R Core Team. *R: A Language and Environment for Statistical Computing (Version 4.2.1*; R Foundation for Statistical Computing: Vienna, Austria https://www.R-project.org/. accessed June 23, 2022.
(59) Diamond, S.; Lavy, A.; Crits-Christoph, A.; Matheus Carnevali, P. B.; Sharrar, A.; Williams, K. H.; Banfield, J. F. Soils and Sediments Host Thermoplasmata Archaea Encoding Novel Copper Membrane Monooxygenases (CuMMOs). *ISME J.* **2022**, *16* (5), 1348−1362.
(60) Crozier, T. E.; Yamamoto, S. Solubility of Hydrogen in Water, Sea Water, and Sodium Chloride Solutions. *J. Chem. Eng. Data* **1974**, *19* (3), 242−244.
(61) Löffler, F. E.; Tiedje, J. M.; Sanford, R. A. Fraction of Electrons Consumed in Electron Acceptor Reduction and Hydrogen Thresholds as Indicators of Halorespiratory Physiology. *Appl. Environ. Microbiol.* **1999**, *65* (9), 4049−4056.
(62) He, J.; Ritalahti, K. M.; Yang, K.-L.; Koenigsberg, S. S.; Löffler, F. E. Detoxification of Vinyl Chloride to Ethene Coupled to Growth of an Anaerobic Bacterium. *Nature* **2003**, *424* (6944), 62−65.
(63) Yan, J.; Şimşir, B.; Farmer, A. T.; Bi, M.; Yang, Y.; Campagna, S. R.; Löffler, F. E. The Corrinoid Cofactor of Reductive Dehalogenases Affects Dechlorination Rates and Extents in Organohalide-Respiring *Dehalococcoides Mccartyi*. *ISME J.* **2016**, *10* (5), 1092−1101.
(64) Fincker, M.; Spormann, A. M. Biochemistry of Catabolic Reductive Dehalogenation. *Annu. Rev. Biochem.* **2017**, *86* (1), 357−386.
(65) Sun, Z.; Geng, D.; Zhang, C.; Chen, J.; Zhou, X.; Zhang, Y.; Zhou, Q.; Hoffmann, M. R. Vitamin B12 (CoII) Initiates the Reductive Defluorination of Branched Perfluorooctane Sulfonate (Br-PFOS) in the Presence of Sulfide. *Chem. Eng. J.* **2021**, *423*, No. 130149.
(66) Liu, J.; Van Hoomissen, D. J.; Liu, T.; Maizel, A.; Huo, X.; Fernández, S. R.; Ren, C.; Xiao, X.; Fang, Y.; Schaefer, C. E.; Higgins, C. P.; Vyas, S.; Strathmann, T. J. Reductive Defluorination of Branched Per- and Polyfluoroalkyl Substances with Cobalt Complex Catalysts. *Environ. Sci. Technol. Lett.* **2018**, *5* (5), 289−294.
(67) Cheng, H.; Cheng, D.; Mao, J.; Lu, T.; Hong, P.-Y. Identification and Characterization of Core Sludge and Biofilm Microbiota in Anaerobic Membrane Bioreactors. *Environ. Int.* **2019**, *133*, No. 105165.
(68) Cai, Y.; Chen, H.; Yuan, R.; Wang, F.; Chen, Z.; Zhou, B. Metagenomic Analysis of Soil Microbial Community under PFOA and PFOS Stress. *Environ. Res.* **2020**, *188*, No. 109838.
(69) Muñoz-Duarte, L.; Chakraborty, S.; Grøn, L. V.; Bambace, M. F.; Catalano, J.; Philips, J. H_2 Consumption by Various Acetogenic Bacteria Follows First-Order Kinetics up to H_2 Saturation *bioRxiv* 2024 DOI: 10.1101/2024.05.08.593002.
(70) Yang, Y.; Schubert, T.; Lv, Y.; Li, X.; Yan, J. Comparative Genomic Analysis Reveals Preserved Features in Organohalide-Respiring *Sulfurospirillum* Strains. *mSphere* **2022**, *7* (1), No. e00931−21.
(71) Kruse, S.; Goris, T.; Westermann, M.; Adrian, L.; Diekert, G. Hydrogen Production by Sulfurospirillum Species Enables Syntrophic Interactions of Epsilonproteobacteria. *Nat. Commun.* **2018**, *9* (1), No. 4872.
(72) Marquis, R. E.; Clock, S. A.; Mota-Meira, M. Fluoride and Organic Weak Acids as Modulators of Microbial Physiology. *FEMS Microbiol. Rev.* **2003**, *26* (5), 493−510.
(73) Dodge, A. G.; Thoma, C. J.; O'Connor, M. R.; Wackett, L. P. Recombinant *Pseudomonas* Growing on Non-Natural Fluorinated Substrates Shows Stress but Overall Tolerance to Cytoplasmically Released Fluoride Anion. *mBio* **2024**, *15* (1), No. e02785−23.
(74) Qin, J.; Chai, G.; Brewer, J. M.; Lovelace, L. L.; Lebioda, L. Fluoride Inhibition of Enolase: Crystal Structure and Thermodynamics. *Biochemistry* **2006**, *45* (3), 793−800.
(75) Rapp, M.; Granseth, E.; Seppälä, S.; Von Heijne, G. Identification and Evolution of Dual-Topology Membrane Proteins. *Nat. Struct. Mol. Biol.* **2006**, *13* (2), 112−116.
(76) Abramson, J.; Adler, J.; Dunger, J.; Evans, R.; Green, T.; Pritzel, A.; Ronneberger, O.; Willmore, L.; Ballard, A. J.; Bambrick, J.; Bodenstein, S. W.; Evans, D. A.; Hung, C.-C.; O'Neill, M.; Reiman, D.; Tunyasuvunakool, K.; Wu, Z.; Žemgulytė, A.; Arvaniti, E.; Beattie, C.; Bertolli, O.; Bridgland, A.; Cherepanov, A.; Congreve, M.; Cowen-Rivers, A. I.; Cowie, A.; Figurnov, M.; Fuchs, F. B.; Gladman, H.; Jain, R.; Khan, Y. A.; Low, C. M. R.; Perlin, K.; Potapenko, A.; Savy, P.; Singh, S.; Stecula, A.; Thillaisundaram, A.; Tong, C.; Yakneen, S.; Zhong, E. D.; Zielinski, M.; Žídek, A.; Bapst, V.; Kohli, P.; Jaderberg, M.; Hassabis, D.; Jumper, J. M. Accurate Structure Prediction of Biomolecular Interactions with AlphaFold 3. *Nature* **2024**, *630* (8016), 493−500.
(77) Stockbridge, R. B.; Kolmakova-Partensky, L.; Shane, T.; Koide, A.; Koide, S.; Miller, C.; Newstead, S. Crystal Structures of a Double-Barrelled Fluoride Ion Channel. *Nature* **2015**, *525* (7570), 548−551.
(78) Ubarretxena-Belandia, I. Three-Dimensional Structure of the Bacterial Multidrug Transporter EmrE Shows It Is an Asymmetric Homodimer. *EMBO J.* **2003**, *22* (23), 6175−6181.
(79) Yagi, T. Bacterial NADH-Quinone Oxidoreductases. *J. Bioenerg. Biomembr.* **1991**, *23* (2), 211−225.
(80) Efremov, R. G.; Baradaran, R.; Sazanov, L. A. The Architecture of Respiratory Complex I. *Nature* **2010**, *465* (7297), 441−445.
(81) Porra, R.; Jones, O. Studies on Ferrochelatase. 2. An in Vestigation of the Role Offerrochelatase in the Biosynthesis of Various Haem Prosthetic Groups. *Biochem. J.* **1963**, *87* (1), 186−192.